Influence of surface treatment and interface layers on electrical spin injection efficiency and transport in InAs

L. Zhu and E. T. Yu[a)]
Department of Electrical and Computer Engineering, Microelectronics Research Center, The University of Texas at Austin, Austin, Texas 78758

(Received 30 June 2010; accepted 20 September 2010; published 20 October 2010)

Spin-valve, weak localization/antilocalization, and scanned probe microscopy measurements are used to investigate the influence of sulfur-based surface treatments and electrically insulating barrier layers on spin injection into, and spin transport within, the two-dimensional electron layer at the surface of *p*-type InAs at 4.2 K. An electrically insulating barrier layer is found to be required to achieve nonzero spin injection efficiency, with a 3 nm Al_2O_3 electrically insulating barrier providing a spin injection efficiency of $5 \pm 2\%$. Conductive atomic force microscopy suggests that localized leakage through the InAs native oxide is sufficient to suppress spin-polarized current injection in the absence of a more highly insulating barrier layer. Spin scattering lengths are determined experimentally from both weak localization/antilocalization and spin-valve measurements. Spin and elastic scattering lengths of 230 ± 20 and 85 ± 5 nm, respectively, are measured, with a sulfur-based surface treatment increasing the spin scattering length to 250 ± 20 nm and decreasing the elastic scattering length to 65 ± 5 nm. © *2010 American Vacuum Society.* [DOI: 10.1116/1.3502674]

I. INTRODUCTION

All-electrical spintronic devices based on ferromagnet/semiconductor hybrid structures offer the potential for realization of logic and switching performance with high speed and low power consumption, and the possibility to integrate additional functionalities such as nonvolatile information storage with more conventional semiconductor electronics.[1] Structures incorporating narrow-bandgap semiconductors offer potential advantages for spintronic device applications due to their combination of high electron mobility and strong spin-orbit coupling,[2] but only limited information is available concerning spin injection into and spin transport within the surface electron layer of InAs (Ref. 3) compared to that reported for GaAs (Refs. 4 and 5) or GaAs/InGaAs/InAlAs quantum-well structures.[6,7] InAs is of particular interest as it offers the advantages of a strong Rashba effect[8,9] for coupling of electron spin transport to transverse electric field for spin transistor devices,[10] and the inherent presence of a surface electron layer that facilitates strong coupling of electrons in InAs to a ferromagnetic contact.[11,12]

We describe here the effect of InAs surface processing and interfacial layer insertion within a ferromagnet/InAs contact on electrical spin injection efficiency and on elastic scattering and spin dephasing lengths within the surface electron layer of *p*-type InAs. Spin injection efficiencies and spin diffusion lengths are determined using magnetoresistance measurements on spin-valve structures with variable channel lengths, with spin diffusion lengths corroborated and scattering lengths determined by analysis of weak localization/antilocalization behavior in Corbino disk structures. Our studies indicate that insertion of a thin insulating layer, in this case Al_2O_3, is required to achieve injection of current with measurable spin polarization from a Co contact into the *p*-type InAs surface electron layer, and that InAs surface passivation improves the spin diffusion length and decreases the transport scattering length in the InAs surface electron layer.

II. EXPERIMENT

Spin-valve and Corbino disk structures were fabricated on lightly doped *p*-type InAs (100) wafers, as shown schematically in Fig. 1. Also shown in this figure is a schematic energy band-edge diagram illustrating formation of an electron inversion layer at the InAs surface due to pinning of the Fermi level above the conduction band-edge.[13] Hall measurements performed on the *p*-type InAs wafers provided confirmation that, at temperatures below 77 K, the surface electron layer is electrically isolated from the *p*-type InAs bulk carriers, and yielded a mobility of $\sim 6000\ cm^2/V\,s$ and electron sheet concentration of $\sim 1 \times 10^{12}\ cm^{-2}$ at 4 K for the surface electron layer.

Both spin-valve and Corbino disk structures were fabricated using a standard lift-off process, with one of the two approaches employed to control the electronic properties of the Co/InAs interface. In the first, 35 nm Co metallization was deposited by electron beam evaporation on InAs cleaned with acetone and then isopropanol with ultrasonic agitation for 3 min each. This was assumed to result in an interface with the Co and InAs layers separated by the native oxide formed on the InAs surface.[14] In the second, the InAs surface was first cleaned in organic solvents as above and then soaked for 15 min at 35 °C in 7% $(NH_4)_2S$ in which extra sulfur was dissolved to form a sulfur-saturated solution. This latter process has been shown previously to result in removal of the native oxide and formation of In–S bonds at the InAs surface.[14] Approximately 3 nm of Al_2O_3 was then deposited by rf sputtering on the cleaned InAs surface, followed by

[a)]Electronic mail: ety@ece.utexas.edu

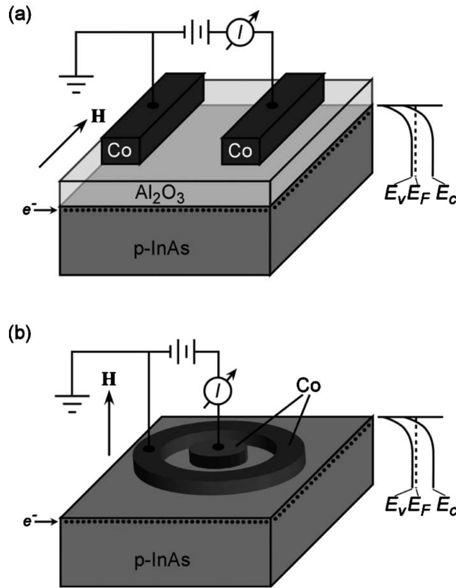

FIG. 1. (a) Schematic diagram of spin-valve device structure as fabricated on p-type InAs, magnetoresistance measurement configuration, and InAs electronic structure. (b) Schematic diagram of Corbino disk device structure, measurement configuration, and InAs electronic structure.

electron beam evaporation of 35 nm Co. Conductive atomic force microscopy (AFM) was used to characterize the electrical conductivity through the native oxide and Al_2O_3 layers and magnetic force microscopy (MFM) to characterize the magnetization state of the Co contacts as a function of external applied magnetic field.

III. RESULTS AND DISCUSSION

A. Nanoscale interface oxide conductance

Figure 2 shows the AFM topographs and conductive AFM images of local current flow through the InAs native oxide present after cleaning in acetone and isopropanol, and

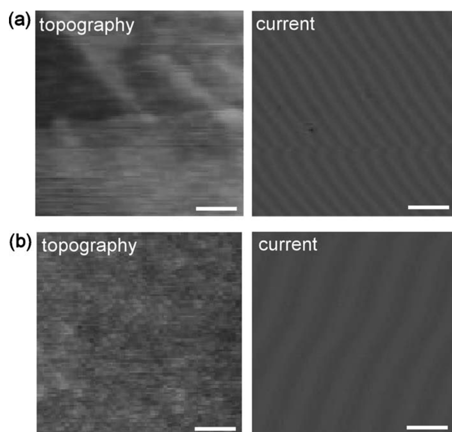

FIG. 2. Topographic and conductive atomic force microscope images, obtained simultaneously in each case with 1 V bias applied to the sample, of (a) p-type InAs with native oxide layer and (b) p-type InAs on which a 3 nm Al_2O_3 layer have been deposited by sputtering. All scale bars are 200 nm. Gray scales correspond to 5 nm for topography, and 1 nA for current.

through a 3 nm Al_2O_3 layer sputtered onto a sulfur-treated InAs surface as described above. The topographic and conductive AFM images were obtained simultaneously in each case, with a bias voltage of 1 V applied to the sample relative to a conductive probe tip. The gray scale in each conductive AFM image corresponds to a range of 0–1 nA. We see in Fig. 2(a) that the native oxide suffers from highly localized current leakage through the oxide at several points. In contrast, no current leakage is observed through the 3 nm Al_2O_3 film into the underlying InAs layer, for bias voltages as high as 5 V. The established significance of a tunnel barrier in enabling injection of spin-polarized current from a ferromagnetic contact into a semiconductor[15] suggests that spin-polarized current injection into a semiconductor is difficult, at best, to achieve through low-resistance interfaces; for a nanoscale spin-valve with the InAs native oxide, the contact resistance is low due to the pinholelike leakage centers in the native oxide, as shown in Fig. 2(a). Therefore, most of the source-drain current through the spin-valve device is likely to be conducted through the localized interface leakage centers without significant spin polarization and the spin-dependent signal of the spin-valve device should be then largely suppressed. In contrast, the presence of an Al_2O_3 layer at the Co–InAs interface eliminates the leakage current flow through the native oxide and should enable spin-polarized current injection into and transport in the spin-valve device.

B. Spin-valve magnetoresistance

The electrical resistance of spin-valve structures fabricated with Al_2O_3 interface layers on p-type InAs was measured at 4.2 K as a function of external magnetic field applied along the width of the Co contacts, as shown schematically in Fig. 1(a). No measurable magnetoresistance was observed for spin-valve devices fabricated with Co contacts deposited directly on as-cleaned or sulfur-passivated p-InAs surfaces. For spin-valve devices fabricated with Al_2O_3 interfacial layers separating the Co contacts from the p-InAs surface, the magnetoresistance MR plotted in Fig. 1(a) is defined as

$$MR \equiv \frac{\Delta R}{R^{\uparrow\uparrow}}, \tag{1}$$

where $R^{\uparrow\uparrow}$ is the average spin-valve resistance for contacts with parallel magnetization over the entire range of applied magnetic fields, and ΔR is the deviation of the resistance from $R^{\uparrow\uparrow}$. MR measured as a function of external applied magnetic field for Co contacts with a center-to-center separation of 300 nm is plotted in Fig. 3(a). The key features of interest are the sharp changes in resistance that occur for applied fields in the vicinity of ± 1000 Oe. These shifts correspond to changes in resistance of 0.12% when the field is swept in the forward (from $-$ to +) direction, and 0.09% when the field is swept in the reverse (from + to $-$) direction. Figure 3(b) shows the measured resistance change, on a logarithmic scale, as a function of channel length, i.e., center-to-center separation between the Co contacts in the

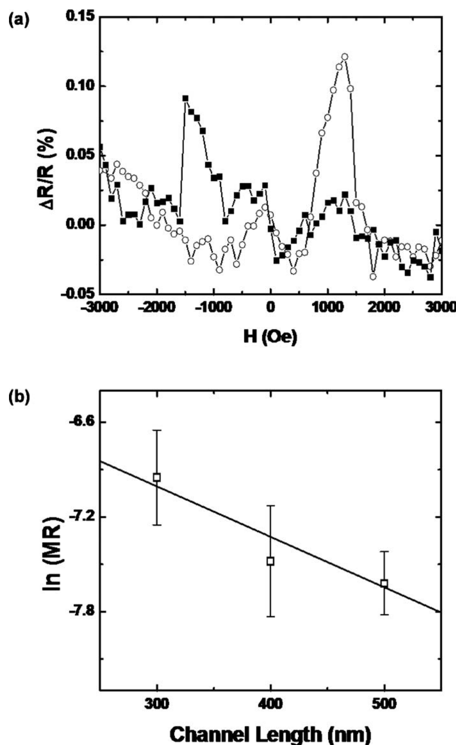

FIG. 3. (a) Magnetoresistance measured for spin-valve device structure shown in Fig. 1(a), for field sweep directions from − to + (open circles) and from + to − (solid squares). (b) Maximum measured magnetoresistance as a function of spin-valve channel length (filled squares), along with curve fitted according to Eq. (1) from which the spin injection efficiency and spin diffusion length are determined.

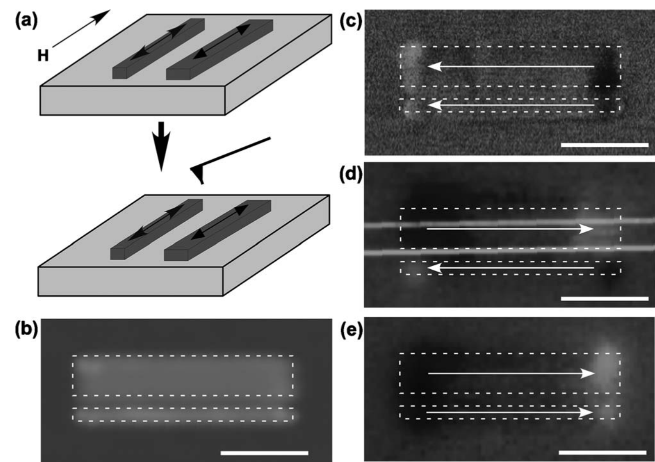

FIG. 4. (a) Schematic diagram of measurement process for atomic and magnetic force microscopy of Co ferromagnetic contacts for spin-valve device. (b) Topographic image of Co contacts and [(c)–(e)] magnetic force images of Co contacts after application of external magnetic fields of 300, 600, and 1200 Oe, respectively. The magnetic force images show the transition from parallel magnetization, in (c), to antiparallel magnetization, in (d), and back to parallel magnetization, in (e), in the opposite direction to that in (c). All scale bars are 500 nm. Gray scale corresponds to 300 nm in topographic image. The dashed outlines indicate the edges of the Co contacts. The magnetization direction of each Co contact is indicated by arrows.

direction of carrier transport, in several spin-valve structures. The magnetoresistance is seen to vary exponentially with channel length, as expected for spin-dependent electron transport within a semiconductor channel. Specifically, the magnetoresistance is expected to be given by[16]

$$MR \equiv \frac{\Delta R}{R^{\uparrow\uparrow}} = \frac{\gamma^2}{1-\gamma^2} e^{-l_c/l_{sf}}, \qquad (2)$$

where γ is the spin polarization of the current injected from the Co contact into the semiconductor, l_c is the spin-valve channel length, and l_{sf} is the spin diffusion length in the semiconductor channel. Analysis of the data in Fig. 3(b) using the functional dependence given in Eq. (2) yields a spin diffusion length l_{sf} of 310 ± 130 nm, and a spin injection efficiency γ of $5 \pm 2\%$ at 4.2 K.

To confirm that these observed shifts in resistance correspond to changes in the relative magnetization of the two Co contacts constituting the spin-valve structure, MFM measurements were performed as a function of externally applied magnetic field at ambient temperature on Co contact structures identical to those employed in the resistance measurements, as shown schematically in Fig. 4(a). Figure 4(b) shows an AFM topographic image of the Co contact structures, and Figs. 4(c)–4(e) shows the MFM images after application of external magnetic fields of 300, 600, and 1200 Oe. The figure reveals a clear transition from parallel magnetization, in Fig. 4(c), to antiparallel magnetization, in Fig. 4(d), at 600 Oe, and back to parallel magnetization, but in the opposite direction, in Fig. 4(e), at 1200 Oe. The magnetic fields at which spin-dependent changes in resistance are observed in the low-temperature device measurements shown in Fig. 3 are somewhat larger, which is as expected based on the known temperature dependence of the coercivity of Co thin films.[17]

C. Weak localization and antilocalization

To verify that parasitic magnetoresistance effects such as anisotropic magnetoresistance and the local Hall effect[18–20] were not influencing the determination of the electron spin diffusion length, and to obtain additional information concerning transport scattering lengths, we examine weak localization/antilocalization measurements performed on Corbino disk structures fabricated on *p*-type InAs, with a 20 μm inner diameter and 40 μm outer diameter, as illustrated schematically in Fig. 1(b). The classic Drude parabolas[21] are observed in measured magnetoconductance characteristics at high magnetic fields and subtracted from initial magnetoconductance characteristics. The remaining magnetoconductance features are due to the weak localization and antilocalization quantum corrections to classic Drude models.

The Hikami-Larkin-Nagaoka theory fitted to the corrected magnetoconductance characteristics provides information about elastic, inelastic, and spin scattering lengths[22] and has also been used to analyze spin-orbit coupling in GaAs and in InAs inversion layers.[23,24] However, it fails to achieve an appropriate fit in some cases, for example, InAs inversion layers in Ref. 24 since it only includes only the Elliot–Yafet spin relaxation mechanism and not the Dyakonov-Perel

mechanism, the dominant mechanism in the two-dimensional electron system in III-V semiconductors with a cubic crystal structure. In comparison, the Iordanskii–Lynda–Geller–Pikus (ILP) theory accounts for both of these spin relaxation mechanisms[25,26] and provides a much better description of the magnetoconductance characteristics measured in InAs surface electron layers.[27] Furthermore, for transport in the InAs surface inversion layer, since Rashba effects due to structural inversion asymmetry dominate the spin relaxation,[28] the ILP theory can be simplified by neglecting Elliot–Yafet spin relaxation and spin-orbit scattering from bulk inversion asymmetry. Thus, in fitting the ILP theory to experimental data, in Eqs. (37) and (38) from Ref. 26, the third order spin precession term Ω_3 is taken to be zero, and the remaining first order spin precession term Ω_1 is replaced by $\Omega_1^{(2)}$, the term determined by Rashba effects.

The characteristic fields B_α for elastic, inelastic, and spin-orbit scattering are then determined by fitting measured magnetoconductance characteristics to the simplified ILP theory and can be related to the corresponding scattering times according to

$$B_\alpha = \frac{h}{4De\tau_\alpha}, \tag{3}$$

where α denotes the elastic, inelastic, or spin-orbit scattering and D is the electron diffusion constant, given by $D = (1/2)v_f^2\tau_e$. v_f is the electron Fermi velocity, determined to be 1.0×10^8 cm/s from the relationship[29]

$$v_f = \frac{\hbar\sqrt{2\pi n_s}}{m^*}. \tag{4}$$

Figure 5(a) shows measured magnetoconductance characteristics for a Corbino disk device with the InAs native oxide present on the surface between the contacts, along with the fitted curves based on the ILP theory. Figure 5(b) shows magnetoconductance characteristics of a Corbino disk device for which the exposed InAs surface was treated with a sulfur-containing solution, along with the fitted curves based on the ILP theory. With the native oxide present, the analysis based on ILP theory yields elastic and spin-orbit scattering lengths $l_e = 85\pm5$ and $l_{so} = 220\pm20$ nm, respectively, and elastic and spin-orbit scattering lengths $l_e = 65\pm5$ and $l_{so} = 250\pm20$ nm after surface treatment.

We interpret these results as follows: the sulfur-passivation removes the InAs native oxide layers, thereby suppressing the spin-orbit relaxation from oxygen scattering centers in the InAs native oxide with paramagnetic nature,[30] and eliminates surface states from the bandgap to improve the electrical properties of InAs surface electron layers.[31] However, it may also create a rougher surface and thereby reduce the scattering lengths.[32] Surface scattering is influenced by both the density of surface scattering centers and surface roughness, and it is difficult therefore to assess definitively the effects of sulfur-passivation on the scattering lengths. Hall measurements have shown that carrier densities increase after sulfur-passivation and are consistent with stronger band bending at the surface.[14] Higher carrier densities introduce more electron-electron scattering at lower temperature and eventually reduce the elastic scattering length, which is consistent with our measurements. We also note that the Rashba coefficient decreases with increasing carrier densities,[27] which implies reduced spin-orbit coupling through Rashba effects, and thus a longer spin-orbit scattering length. We speculate that the reduction of the elastic scattering length and the increase in the spin-orbit scattering length arise from the combination of these effects. In addition, we note that the spin-orbit scattering lengths l_{so} obtained from these measurements are in reasonable agreement with the spin diffusion length l_{sf} determined from spin-valve measurements, as described in Sec. III B.

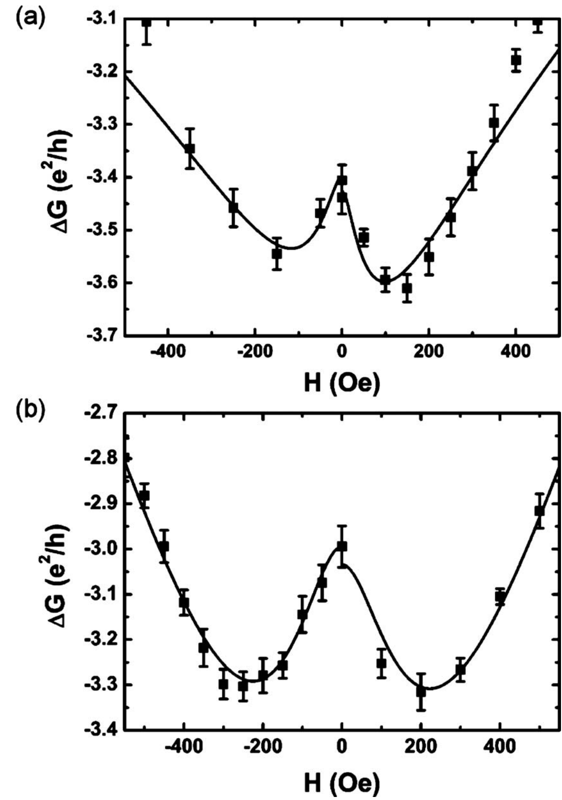

FIG. 5. Magnetoconductance measured in Corbino disk device structure shown in Fig. 1(b), along with fitted curves from ILP theory, for (a) Corbino disk device with native oxide on InAs surface and (b) Corbino disk device with sulfur-passivated InAs surface.

IV. CONCLUSIONS

We have used a combination of spin-valve electrical measurements, weak localization/antilocalization measurements and analysis, and scanned probe microscopy to assess the influence of interfacial layers and surface treatments on spin-polarized current injection from Co contacts into p-type InAs, and spin-polarized electron transport within the two-dimensional electron layer at the InAs surface. The presence of an electrically insulating tunnel barrier at the interface between the Co contact and InAs surface was found to be essential to observation of nonzero spin injection efficiency, with a 3 nm Al_2O_3 interface barrier yielding a spin injection

efficiency of 5 ± 2%. Spin-valve and weak localization/antilocalization measurements at 4.2 K yielded consistent spin scattering lengths in the range ~250 nm. A sulfur-based surface treatment was found to increase the spin scattering length by 14% and reduce the elastic scattering length by 24%. These measurements provide both insight into spin injection and transport processes for the surface electron layer in InAs, and guidance in the design of electronic and spintronic devices based on spin-dependent and/or ballistic electron transport in the InAs surface electron layer.

ACKNOWLEDGMENT

Part of this work was supported by the Office of Naval Research (Grant No. N00014-02-1-1016).

[1] I. Žutić, J. Fabian, and S. Das Sarma, Rev. Mod. Phys. **76**, 323 (2004).
[2] A. W. Cummings, R. Akis, and D. K. Ferry, Appl. Phys. Lett. **89**, 172115 (2006).
[3] T. Matsuyama, C.-M. Hu, D. Grundler, G. Meier, and U. Merkt, Phys. Rev. B **65**, 155322 (2002).
[4] B. T. Jonker, S. C. Erwin, A. Petrou, and A. G. Petukhov, MRS Bull. **28**, 740 (2003).
[5] T. Inokuchi, T. Marukame, M. Ishikawa, H. Sugiyama, and Y. Saito, Appl. Phys. Express **2**, 023006 (2009).
[6] Y. D. Park, B. T. Jonker, B. R. Bennett, G. Itskos, M. Furis, G. Kioseoglou, and A. Petrou, Appl. Phys. Lett. **77**, 3989 (2000).
[7] H. C. Koo, H. Yi, J. B. Ko, J. Chang, S. H. Han, D. Jung, S. G. Huh, and J. Eom, Appl. Phys. Lett. **90**, 022101 (2007).
[8] D. Grundler, Phys. Rev. Lett. **84**, 6074 (2000).
[9] T. Matsuyama, R. Kürsten, C. Meißner, and U. Merkt, Phys. Rev. B **61**, 15588 (2000).
[10] S. Datta and B. Das, Appl. Phys. Lett. **56**, 665 (1990).
[11] J. P. McGuire, C. Ciuti, and L. J. Sham, Phys. Rev. B **69**, 115339 (2004).
[12] K. Yoh, H. Ohno, Y. Katano, K. Mukasa, and M. Ramsteiner, J. Cryst. Growth **251**, 337 (2003).
[13] L. O. Olsson, C. B. M. Andersson, M. C. Hakansson, J. Kanski, L. Ilver, and U. O. Karlsson, Phys. Rev. Lett. **76**, 3626 (1996).
[14] D. Y. Petrovykh, M. J. Yang, and L. J. Whitman, Surf. Sci. **523**, 231 (2003).
[15] G. Schmidt, D. Ferrand, L. W. Molenkamp, A. T. Filip, and B. J. van Wees, Phys. Rev. B **62**, R4790 (2000).
[16] A. Fert, J.-M. George, H. Jaffrès, and R. Mattana, IEEE Trans. Electron Devices **54**, 921 (2007).
[17] J. P. Lazzari, I. Melnicr, and D. Randet, IEEE Trans. Magn. **3**, 205 (1967).
[18] F. G. Monzon, M. Johnson, and M. L. Roukes, Appl. Phys. Lett. **71**, 3087 (1997).
[19] F. G. Monzon, D. S. Patterson, and M. L. Roukes, J. Magn. Magn. Mater. **195**, 19 (1999).
[20] F. G. Monzon and M. L. Roukes, J. Magn. Magn. Mater. **198–199**, 632 (1999).
[21] N. W. Ashcroft and N. D. Mermin, *Solid State Physics* (Holt, Rinehart and Winston, New York, 1976), Chap. 1, pp. 12–14.
[22] S. Hikami, A. I. Larkin, and Y. Nagaoka, Prog. Theor. Phys. **63**, 707 (1980).
[23] P. D. Dresselhaus, C. M. A. Papavassiliou, R. G. Wheeler, and R. N. Sacks, Phys. Rev. Lett. **68**, 106 (1992).
[24] Y. Kawaguchi, I. Takayanagi, and S. Kawaji, J. Phys. Soc. Jpn. **56**, 1293 (1987).
[25] S. V. Iordanskii, Y. B. Lynda-Geller, and G. E. Pikus, JETP Lett. **60**, 206 (1994).
[26] W. Knap *et al.*, Phys. Rev. B **53**, 3912 (1996).
[27] C. Schierholz, T. Matsuyama, U. Merkt, and G. Meier, Phys. Rev. B **70**, 233311 (2004).
[28] S. Lamari, Phys. Rev. B **64**, 245340 (2001).
[29] S. Datta, *Electronic Transport in Mesoscopic Systems* (Cambridge University Press, Cambridge, 1995), Chap. 1, p. 17.
[30] S. Gardelis, C. G. Smith, C. H. W. Barnes, E. H. Linfield, and D. A. Ritchie, Phys. Rev. B **60**, 7764 (1999).
[31] V. N. Bessolov and M. V. Lebedev, Semiconductors **32**, 1141 (1998).
[32] Q. Hang, F. Wang, P. D. Carpenter, D. Zemlyanov, D. Zakharov, E. A. Stach, W. E. Buhro, and D. B. Janes, Nano Lett. **8**, 49 (2008).